Science of the Total Environment 944 (2024) 173728

Contents lists available at ScienceDirect

Science of the Total Environment

journal homepage: www.elsevier.com/locate/scitotenv

Assessing urban heat island mitigation potential of realistic roof greening across local climate zones: A highly-resolved weather research and forecasting model study

Mitali Yeshwant Joshi [a,b,*], Jacques Teller [a]

[a] LEMA Research Group, Urban & Environmental Engineering Department, University of Liège, B52, Allee de la Decouverte, 9, Liege 4000, Belgium
[b] Copernicus Institute of Sustainable Development - Utrecht University, Princetonlaan 8a, Utrecht 3584 CB, the Netherlands

HIGHLIGHTS

- UHI mitigation studies use unrealistic (uniform or 100 %) green roof (GR) fractions.
- Impact of realistic GR fraction in LCZs on UHI effect is studied at regional scale.
- WRF with BEP + BEM parameterisation was used with LCZ classification as land use.
- Realistic roof greening is not sufficient to significantly reduce the UHI effect, regionally.
- Decrease in temperatures depends on the urban morphology and GR fractions in LCZs.

GRAPHICAL ABSTRACT

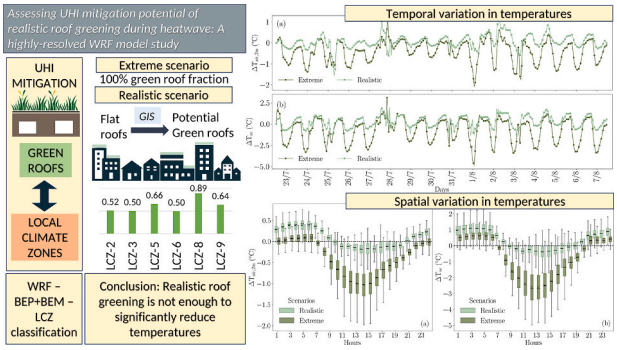

ARTICLE INFO

Editor: Shuqing Zhao

Keywords:
Urban heat island
Green roofs
WRF
Local climate zones
Heatwave
GIS

ABSTRACT

Given their multifold benefits, green roofs are often considered to mitigate the urban heat island (UHI) effect. Most mesoscale studies consider 100 % green roof fraction or the same green roof fraction in each urban land use category while analysing the influence of green roofs on the UHI effect, which can overestimate their impact on UHI. Consequently, the impact of green roofs evaluated in these studies may not be suitable for informing policy decisions. Furthermore, the effect of morphologies on temperature reduction due to green roofs has not been previously studied. To address this gap, in this paper, we evaluate the impact of a realistic fraction of green roofs specific to the respective local climate zones (LCZ) on the UHI effect during a heatwave in Liège, Belgium, employing a high-resolution WRF study using the BEP-BEM parameterisation with LCZ land use classification. The realistic fraction is estimated for every LCZ class based on the average percentage of flat roofs observed in each LCZ class in Liège. Accordingly, distinct realistic fractions of green roofs are assigned to each LCZ class in WRF. We run the WRF simulation for the base scenario (without green roofs), extreme scenario (100 % green roof fraction), and realistic scenario. The results indicate a limited reduction in near-surface air and surface temperature in a realistic scenario, with a nighttime increase in temperature. Additionally, in the extreme scenario, the temperature reduction largely depends on the morphology. However, in a realistic scenario, it depends on the green roof fraction. Other indicators like heat index and UHI intensity also are not reduced considerably

* Corresponding author at: Copernicus Institute of Sustainable Development - Utrecht University, Princetonlaan 8a, Utrecht 3584 CB, the Netherlands.
E-mail addresses: mjoshi@uliege.be (M.Y. Joshi), jacques.teller@uliege.be (J. Teller).

https://doi.org/10.1016/j.scitotenv.2024.173728
Received 8 January 2024; Received in revised form 29 May 2024; Accepted 1 June 2024
Available online 10 June 2024

with realistic greening. Therefore, realistic roof greening alone will not be sufficient to achieve an impact on a city-scale.

1. Introduction

Climate change is causing frequent and extreme heat events such as heat waves, resulting in high heat-stress-induced mortality and increased energy consumption in urban areas (Wang et al., 2022; Patz et al., 2005; Gabriel and Endlicher, 2011). Moreover, with unprecedented urbanisation, urban areas are experiencing higher temperatures compared to their rural counterparts, causing the urban heat island (UHI) effect. Heat waves could exacerbate the impacts of the UHI effect (Li and Bou-Zeid, 2013; Chew et al., 2021) by altering the sensible and latent heat flux asymmetrically (Li et al., 2015) and changing the wind speeds (Li et al., 2016). Therefore, mitigation of the impacts of heat waves and the UHI effect is crucial.

Several mitigation strategies have been proposed to reduce the extreme impacts of heat waves, such as green-blue infrastructure (Gunawardena et al., 2017), green spaces (Santamouris et al., 2018; Li and Liu, 2021) and cool reflective materials (Santamouris et al., 2011; Liu et al., 2022). Compared to usual mitigation strategies such as trees, water ponds, or parks, roof-based strategies such as green roofs and cool roofs are gaining more popularity in urban areas (Li et al., 2014; He et al., 2020; Liu et al., 2022; Sharma et al., 2016) due to the lack of other free spaces. Moreover, since the roofs also receive large amounts of solar radiation, the roof-based strategies can reduce the effects of heat (Li et al., 2014; He et al., 2020). Unlike cool roofs, green roofs provide multiple ecosystem services such as UHI mitigation, enhancing urban biodiversity, stormwater management, and quality of life (Berardi et al., 2014; Joshi and Teller, 2021). Thus, retrofitting green roofs on the building roofs could be a logical strategy, given the additional benefits.

The advantages of green roofs have been convincingly demonstrated at a building or neighbourhood scale (Joshi and Teller, 2021). However, the translation of the mitigation potential of green roofs at these scales to city scale is complex and challenging because of the influence of surface heterogeneity on local microclimate (Li et al., 2014; Yang and Bou-Zeid, 2019; Bou-Zeid et al., 2007). Moreover, the impacts of individual building green rooftops on air temperatures outside the urban canopy may not be captured (Li et al., 2014; Tan et al., 2023). In this aspect, numerical weather prediction (NWP) models aid in upscaling and quantifying the impacts of green roofs at a city or regional scale.

Several studies have used the NWP model, such as the weather research and forecasting (WRF) model, to assess the influence of green roofs on the UHI effect during extreme heat events (Synnefa et al., 2008; Li et al., 2014; Li and Norford, 2016; Sun et al., 2016; Morini et al., 2018). Urban canopy parameterisations in NWP models require the most detailed input data, such as land cover and urban morphology, to appropriately capture the study area's urbanisation. Regional scale data on urban morphology is challenging to obtain but is crucial in improving the modelling capacity. LCZs, defined by Stewart and Oke (2012), facilitate the incorporation of urban morphology into the complex modelling of WRF. LCZs are homogenous regions in terms of surface cover, structure, material and human activity that stretch over hundreds of meters to several kilometres horizontally. After the pioneering work of Brousse et al. (2016) and Martilli et al. (2016), more studies are utilising LCZ maps for defining the urban morphology and surface thermal characteristics within the WRF model (Ribeiro et al., 2021). However, very few studies (Tan et al., 2023; Lu et al., 2023; Kalogeri et al., 2023) have utilised the WRF model with LCZ classes as land use classification for analysing the impact of green roofs on the UHI effect. In this paper, we utilise the WRF model with LCZ classes to describe the urban morphology and characteristics of the study area.

Apart from this, most WRF studies investigate the potential of green roofs at their maximum capacity (100 % green roof fraction) in mitigating the UHI effect (Tan et al., 2023; Liu et al., 2022; Wang et al., 2022; Tewari et al., 2019). 100 % green roof scenarios are unrealistic, especially in European cities where many buildings may have sloped roofs. It is possible to install green roofs on sloped roofs; however, the installation and maintenance costs for this are extremely high (Grunwald et al., 2017; Karteris et al., 2016; Santos et al., 2016). Installing them on flat roofs is more feasible. In order to model the effect of green roofs at a city scale in a plausible way, however, WRF studies should combine both realistic fractions of green roofs and LCZs. By realistic, we mean the existing flat roofs that may be transformed into extensive green roofs without severely altering the building. WRF studies with realistic roof greening fractions are limited in the literature.

Another assumption in most WRF studies of green roofs is the use of the same green roof fraction across all LCZs. Assuming a similar green roof fraction across different land uses is unrealistic since the type of buildings varies across the land uses and LCZs. For instance, residential buildings mainly have sloped roofs in European cities (Meijer et al., 2009; Da Silva and Vicente, 2013; Ferreira et al., 2020), and since they are privately owned, implementing green roofs on them could be challenging (Marvuglia et al., 2020; Blackhurst et al., 2010). However, installing green roofs on commercial buildings such as malls, industrial buildings, or public buildings like schools or hospitals can be relatively easier since the buildings are often maintained by municipalities (Castleton et al., 2010). Therefore, in this study, we provide a method to assess the impact of a realistic fraction of green roofs estimated for each LCZ class on the UHI effect, which is based on the availability of average flat roofs in each LCZ class, identified using remote sensing. Furthermore, while WRF studies with LCZ classification and BEP–BEM (Building Energy Parameterisation and Building Energy Model; most sophisticated parameterisation setting of WRF. For more details, refer Section 2) parameterisation is available for other parts of the world (Gilabert et al., 2021; Liu and Morawska, 2020; Mughal et al., 2020; Tan et al., 2023), such a study has never been employed for North-Western European cities with temperate climates to assess the role of green roofs or any other mitigation strategy. These cities are experiencing recurring severe heat waves with a longer duration each passing year during summer (Doutreloup et al., 2022). Therefore, assessing the potential of mitigation measures like green roofs in such cities is necessary. Consequently, we perform this study in the context of Liège, Belgium.

Essentially, in this paper, we perform a high-resolution WRF study using the BEP-BEM parameterisation with LCZ land use classification to assess the impact of a realistic fraction of green roofs in each LCZ class on the UHI effect during a heatwave in Liège City. There are three main novelties in the paper:

1. By using a fraction of flat roofs obtained using remote sensing as an indication of potential green roofs specific to each LCZ, we assess the impact of the realistic percentage of potential green roofs in every LCZ on the UHI effect.
2. We do this by analysing the spatial and temporal variability of observed effects in terms of temperature and UHI indicators.
3. We assess the impact of green roofs in different LCZs by evaluating the typological variability of air and surface temperatures.

We mainly run three simulations for the study area; i) without green roofs (base scenario), ii) with a realistic fraction of green roofs (realistic scenario) and iii) with 100 % roof greening for all LCZs (extreme scenario).

The remainder of this paper is organised as follows. Section 2 explains the WRF model along with the BEP-BEM parameterisations and the inputs and outputs from the model in detail. Section 3 presents the

model validation and the results from three simulation runs. Finally, Section 4 draws the concluding remarks of our paper.

2. Methodology

2.1. WRF model

The WRF model is an NWP and atmospheric simulation model intended for both research and operational applications. In this paper, we employ the WRF version 4.4.1. WRF model has a dynamic solver that incorporates compressible and non-hydrostatic Euler equations with several physical and dynamic options designed for regional scale. However, as there is an increasing interest in simulating the urban atmosphere, urban canopy schemes are developed and integrated into WRF due to the complex dynamics of urban climate. Urban canopy schemes such as BEP-BEM are included in WRF as physics options to represent better urban morphology, such as building and street geometry and the surface characteristics such as albedo, emissivity, and urban/vegetation fraction. (Ribeiro et al., 2021).

WRF has three urban canopy parameterisations: Single layer urban canopy model (SLUCM), multi-layered urban canopy model (MLUCM) with building energy parameterisation (BEP), and MLUCM with BEP-BEM (Building energy modelling). The SLUCM assumes infinitely long street canyons that represent urban geometry. The MLUCM BEP model represents more sophisticated urban modelling in WRF. It divides the urban canopy into several vertical layers at various heights. It independently solves fluxes and meteorological variables in each layer, enabling the characterisation of building height distribution in high-density built areas.

Coupling with BEM, using BEP-BEM, WRF models the anthropogenic quantities (including emissions from air conditioners or equipment and indoor-outdoor air exchange) at different heights independently as heat or moisture fluxes. As BEP-BEM is the most sophisticated UCM model, we utilise the BEP-BEM parameterisation in this paper to simulate the diurnal variation of near-surface air temperature $(T_{air,2m})$, surface temperature (T_{se}) and relative humidity (RH_{2m}) over the city. The BEP-BEM model computes the surface momentum, heat exchanges, humidity, and turbulent kinetic energy fluxes to the atmospheric dynamics governing equations. Compared to SLUCM, the BEP-BEM system includes (Salamanca and Martilli, 2010; Ribeiro et al., 2021; Segura et al., 2021):

(a) the 3D urban structure in the model using multiple layers and the origins and skins of momentum and heat in the vertical layers within the urban canopy layer,
(b) the impact of horizontal and vertical surfaces such as roads and walls on the momentum, turbulent kinetic energy and potential temperature,
(c) the shading, reflection and blocking effect of horizontal and vertical surfaces on net solar radiation within the urban canopy layer,
(d) exchange of heat between building walls, rooftops, and floors
(e) heat discharged by people and domestic electrical appliances and
(f) air-conditioning cooling, heating, and ventilation

Advanced urban geometry must be described accurately to evaluate the physical processes within the urban region. In the recent versions of WRF, 11 urban LCZ classifications corresponding to the study area can be integrated with the MLUCP BEP-BEM parameterisation. Many studies have implemented this method to assess the urban climate and also to assess the strategies for regulating the urban climate (Brousse et al., 2016; Zonato et al., 2020; Hammerberg et al., 2018; Patel et al., 2020; McRae et al., 2020; Tan et al., 2023). This study uses the LCZ map for Europe generated by WUDAPT (Demuzere et al., 2019a, 2019b).

2.2. Surface energy balance

The surface energy balance of a surface in WRF is represented by:

$$SW_{net} + LW_{net} + AH = LH + SH + G, \quad (1)$$

where SW_{net} is the net shortwave radiation at the surface, LW_{net} is the net longwave radiation at the surface, AH is the anthropogenic heat flux, LH and SH are the latent and sensible heat fluxes, and G is the ground heat flux. For BEP-BEM, the AH comes from air-conditioning, heat exchanges between building interior and exterior air, and the heat released by equipment and people within the buildings. The BEP-BEM parameterisation does not include the AH from traffic or industry (Ribeiro et al., 2021; Tan et al., 2023).

A traditional roof transfers all net radiation into sensible heat flux and heat entering the building, raising the T_{se} and $T_{air,2m}$. Green roofs lower the net radiation at the roof by predominantly releasing the latent heat flux from the vegetation and soil (Zonato et al., 2021). The green roof modelling in WRF is explained briefly in the next section.

2.3. Modelling of green roofs

WRF parameterises the green roofs with land-surface scheme developed based on de Munck et al. (2013) and Gutierrez (2016), which is recently updated by Zonato et al. (2021). It considers the incoming net radiation, water input from precipitation and irrigation, evapotranspiration from vegetation, heat exchange with the atmosphere, and diffusion of energy and moisture throughout the soil to compute the energy and water budgets. This model is one-dimensional, as horizontal transport and subsurface flows are neglected. The green roof in this WRF version consists of 10 layers (~ 30 cm), with five levels representing the organic matter substrate (8 cm), one level representing the drainage layer (5 cm) and four levels describing the insulation layer (16.6 cm). More details can be found in Zonato et al. (2021).

The latent heat flux (*LE*) from green roofs comprises of evaporation from soil moisture and evapotranspiration through the leaves. The heat transfer between green roof layers is calculated using the Fourier diffusion equation for soil temperature. More details on hydrology and thermodynamics of green roofs can be found in Zonato et al. (2021). In this paper, we use the green roof setting with grass which has an albedo of 0.3 and emissivity of 0.93. In addition to this, the simulated green roofs are kept unirrigated.

2.4. Model set-up

2.4.1. Simulation domain

The study area targets Liège City and the surrounding area centred on 50°38′1.43″ N 5°34′2.96″ E. Four one-way nested domains were used with 150 × 150 grid points in domain 1, and 151 × 151 grid points in domains 2 and 3, respectively and 175 × 175 grid points in domain 4, with a grid spacing of 9, 3, 1, 0.333 km in WRF 4.4.1, respectively (Fig. 1 (a)). The outer domain includes the North Sea and Western Europe, whereas the innermost domain contains the Arrondissement of Liège in the centre, surrounded by the Arrondissement of Tongres, Huy, Waremme, Verviers, along with a small part of South-Limburg in the Netherlands. Arrondissements in Belgium are sub-divisions of provinces. The LCZ classification is substituted as Land-use classification in the innermost domain (d04) by updating the surface parameters for every grid (Fig. 1(b)). The other domains are initialised using MODIS land use data. The innermost domain has 10 urban LCZ categories to enable WRF to utilise detailed urban morphologies for the chosen BEP-BEM parameterisation. The details to integrate the LCZ into WRF can be found in Demuzere et al. (2022).

2.4.2. Parameter settings

In this study, we use the LCZ data produced for Europe by Demuzere

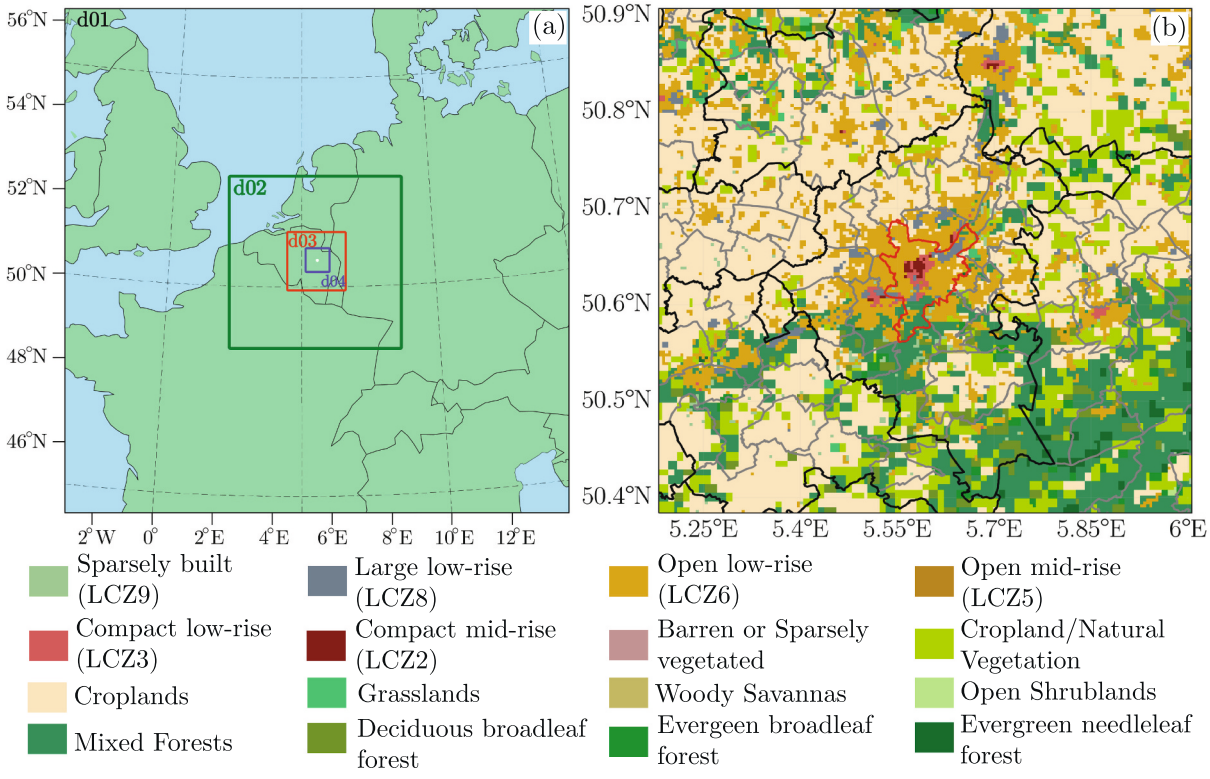

Fig. 1. (a) WRF domain configuration. The outer domain (d01), the second domain (d02), the third domain (d03) and the innermost domain (d04) have a resolution of 9 km, 3 km, 1 km and 333 m, respectively. (b) Urban land-use categories after the incorporation of local climate zones (LCZs) from WUDAPT data over domain d04.(Black borders represent provinces, grey borders represent municipality, red border is the Liège municipal boundary).

et al. (2019a, 2019b) for the innermost domain. The non-urban land covers are based on the MODIS (Moderate Resolution Imaging Spectroradiometer) data 21-class product (Kumar et al., 2014). The innermost domain mainly contains only six urban LCZ classes, which are LCZ-2 (Compact mid-rise), LCZ-3 (Compact low-rise), LCZ-5 (Open midrise), LCZ-6 (Open low-rise), LCZ-8 (Large low-rise), and LCZ-9 (Sparsely built) (Fig. 1(b)). We use 45 vertical levels in Ribeiro et al. (2021) from surface to 50 hPa (Gilabert et al., 2021) with six levels within the urban canopy layer of 5–10 m each. The first point is sufficiently close to the ground (at 2.5 m), which satisfies the requirement of the BEP-BEM model (Gilabert et al., 2021; Broadbent et al., 2020). The integration time-step was 40 s for the outermost domain, and we collected the simulation outputs every hour for the innermost domain.

The initial and boundary conditions were taken from European Centre for Medium-Range Weather Forecasts (ECMWF) reanalysis v5 (ERA5) data (Hersbach et al., 2020) with an update interval of 3 h, because of the higher accuracy and European context. Apart from this, in this work, we used the schemes corresponding to NCAR Convetion permitting physics suite (CONUS), which is reliable and accurate according to the WRF documentation. Particularly, we use the unified Noah land-surface model for the land-surface scheme (Ek et al., 2003; Chen and Dudhia, 2001) and the Thompson microphysics scheme (Thompson and Eidhammer, 2014). We use the Rapid Radiative Transfer Model for Global Circulation Models (RRTMG) for longwave and shortwave radiation (Iacono et al., 2008). For the surface layer scheme we use the Monin-Obukhov-Janjic approach (Janjic, 2002). For the planetary boundary scheme, we changed default scheme to the Bougeault-Lacarrère PBL (BouLac) (Bougeault and Lacarrere, 1989), which is designed to used for urban schemes (Ribeiro et al., 2021). Additionally, no cumulus parameterisation was used (Tan et al., 2023; Zonato et al., 2021). The length and time frame of the simulation is decided based on the occurrence of the most severe and longest heatwave in Liège city. The method used for identifying heatwaves is described in Section 2.4.4.

2.4.3. Realistic potential of green roofs in LCZ

For this study, we estimate a realistic potential of roof greening in Liège city using remote-sensing and geoinformation systems (GIS). We simulate the green roofs only where the existing flat roofs are present to ensure practical greening. We identified flat roofs using LiDAR point cloud data with a point density of 0.8 points/m^2 for Liège. Employing the RANSAC algorithm to process LiDAR point cloud, we obtain the number of planes within a building footprint. Considering flat roofs to have less than a 10° slope, we identify planes that are flat with an area of at least 10 m^2 for each building. This way, we identify the buildings with flat roofs in Liège. The details of this methodology can be found in Joshi et al. (2020). Based on this, we consider buildings with flat roofs for roof greening.

To compute a realistic percentage of green roofs in each LCZ, firstly, we rasterise the building footprint and buildings with green roofs to 1 m resolution raster. We aggregate the pixels to 100 m (same resolution as LCZ) by summing to obtain the proportion of potential green roofs per 100 × 100 m pixels. We calculate a realistic percentage of green roofing in each 100 × 100 m pixel corresponding to LCZ as:

$$GR_{perc} = \frac{GR_{area}}{BU_{area}}, \quad (2)$$

where GR_{area} is the area of potential green roofs in one pixel and BU_{area} is the average of building area in that pixel. We then compute the percentage of green roofs for each LCZ as the average value of the GR_{perc} of the pixels in the selected LCZ. The percentage of roof greening potential is the highest for LCZ-8, followed by LCZ-5, 9, 2, 3 and 6. A figure showing this is provided in the Appendix (Fig. A.1).

2.4.4. Identifying the heatwave

We identify the longest and the most severe heatwave observed in

Liège in the last 20 years to decide the length and time frame of the simulation based on the approach proposed by Ouzeau et al. (2016). This approach is statistical and facilitates consideration of the local climate of the area of interest. The approach is mainly based on high quantiles of distributions of daily temperatures. The heatwave can be characterised for a given period of time using the three settings, namely, *Spic*, *Sdeb and Sint*. *Spic* refers to the temperature threshold beyond which an event is detected, and*Sdeb* is the threshold that defines the beginning and the end of the heatwave. *Sint* is the interruption threshold which enables merging two consecutive occurrences without a significant drop in temperature. These thresholds are 99.5, 97.5 and 95 percentile of the daily average temperature of days in the twenty years (2000−2020). More information on the selection of percentile values can be found in Ouzeau et al. (2016). The meteorological data used for identifying heatwaves is obtained from the weather station nearest to Liège city.

Based on this method, we select the most severe and longest heatwave in Liège to understand the temporal variability of the effect of green roofs on air and surface temperature. Fig. 2(a) shows the intensity and duration of the heatwaves in Liège between 2000 and 2020. We observe that there have been six heatwaves in Liège during this period, and the intensity of heatwaves is increasing with time. Most heatwaves have a duration of more than eight days, and the heatwave of 2018 was the longest heatwave with a severe intensity. Therefore, we choose this heatwave for this work and run the simulation from 23rd July to 7th August. Fig. 2(b) demonstrates the daily mean temperatures for 16 days of this heatwave which was observed from 23rd July to 7th August 2018. The daily mean temperature is the highest for the 27th of July.

The heatwave event starts when the temperature is above the *Sdeb* threshold. The heatwave is interrupted if the daily temperature goes below the *Sdeb* threshold for at least three consecutive days or drops to values below the *Sint* threshold. The values of *Spic*, *Sdeb and Sint*, which are 99.5, 97.5 and 95th percentile, respectively, are computed on the daily mean air temperatures for a given period. These values are a result of a detailed preliminary analysis of EURO-CORDEX data (Ouzeau et al., 2016; Jacob et al., 2013), which led to heatwave identifications close to the application of the operational method. This method is beneficial as it considers the local climate of the study area. We compute the number of heatwaves, their intensity and duration and select the heatwave with the highest intensity and duration. We run the simulation for the entire heatwave in this study.

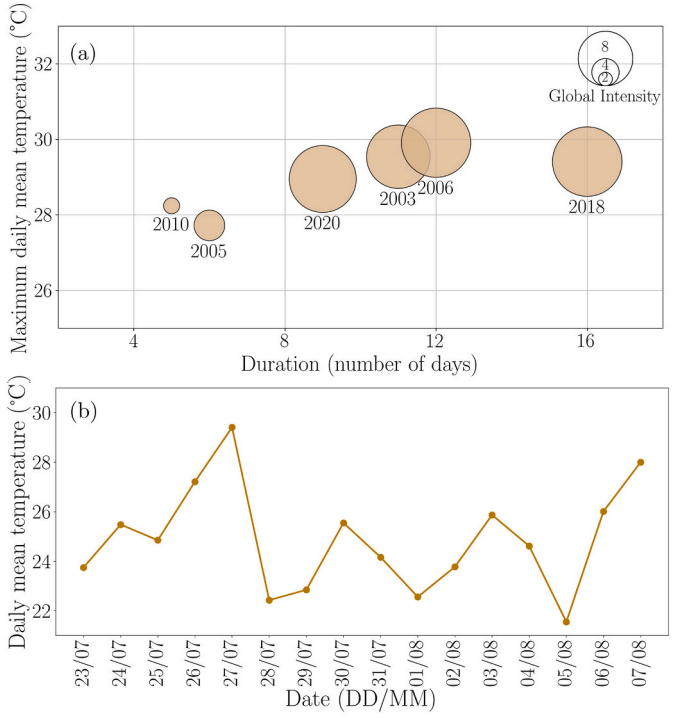

Fig. 2. (a) Intensity and duration of heatwaves in Liège from 2000 to 2020 (b) Daily mean temperature during the longest and most intense heatwave in Liège ((a) is made using the code provided by Joshi et al. (2022); Machard (2022)).

2.5. Indices for assessing UHI effect

2.5.1. Air and surface temperature changes

To assess the impact of green roofs, we present the temporal and spatial differences in air and surface temperature for urban grid cells. The temporal variation is a spatially averaged difference is computed as follows:

$$\Delta T = \frac{\sum_{n=1}^{n} T_{n,base} - T_{n,GR}}{n}, \tag{3}$$

where $T_{n,base}$ is the T_{se} or T_{air} of a grid cell in base scenario and $T_{n,GR}$ is the T_{se} or T_{air} of a grid cell in the scenario with green roofs. n is the number of urban grid cells in the d04 domain.

The temporally averaged spatial variation is computed for 24 h for all the urban grid cells and is computed as follows:

$$\Delta T = \frac{\sum_{n=1}^{n} T_{n,base} - T_{n,GR}}{n} \tag{4}$$

where $T_{n,base}$ is the T_{se} or T_{air} of a grid cell in base scenario and $T_{n,GR}$ is the T_{se} or T_{air} of a grid cell in the scenario with green roofs, for a particular hour. Here, n is the total number of simulated days.

2.5.2. UHI intensity

There are several ways to estimate the UHI intensity (UHII) (Chen et al., 2022; Li et al., 2019; Liao et al., 2018). In this paper, we use the linear equation between urban fraction (Urb_{frac}) and temperature given by Li et al. (2019).

$$UHII_{se/air} = \frac{T_{se/air} - T_{rural,se/air}}{Urb_{frac}}, \tag{5}$$

where $T_{se/air}$ is the air or surface temperature of the urban area and $T_{rural,se/air}$ is the air or surface temperature of the rural area for air or surface UHII, respectively. Here, the Urb_{frac} is the independent variable, and the slope of this equation is the UHII. The intercept, in this case, is the temperature in the non-urban (rural) area. We exclude the areas with open water bodies and consider only the urban LCZ pixels for air and surface temperatures for urban areas. The Urb_{frac} is obtained from LCZ map. This mainly indicates the level of urbanisation with a proportion of impervious areas. With these values, we compute the UHII using Eq. (5).

2.5.3. Heat index

The UHI effect also deteriorates human thermal comfort influencing the health of people. Therefore, we examine heat index (HI) using a regression analysis by Steadman (1979), which is used by many recent studies (Yip et al., 2008; Mohan et al., 2013; Tan et al., 2023). The Steadman's HI is widely used as a metric for measuring thermal comfort that includes temperature and relative humidity. It primarily describes the perception of heat felt by a human body under a given weather. The calculation of HI is as follows (Rothfusz and Headquarters, 1990):

$$\begin{aligned} HI = {} & -42.379 + 2.04901523 \times T + 10.14333127 \times RH - 0.22475541 \times T \times RH \\ & - 0.00683783 \times T^2 - 0.05481717 \times RH^2 + 0.00122874 \times T^2 \times RH \\ & + 0.00085282 \times T \times RH^2 - 0.00000199 \times T^2 \times RH^2 \end{aligned} \tag{6}$$

where the HI is calculated in °F but is transferred to °C for consistency. T is the dry-bulb temperature, and RH is the relative humidity. In our study, the HI was calculated based on $T_{air,2m}$ and RH_{2m} from WRF out-

puts. We also report HT as the difference of HI between base scenario and green roof scenarios (extreme and realistic) as explained in Section 2.5.1.

We also showcase the details of the boundary layer within 2 km by describing the vertical profile of T_{air}, RH and V.

3. Results and discussion

3.1. Comparison of WRF results with meteorological measurements

We validate the values of 2-meter air temperature $(T_{air,2m})$, 2-meter relative humidity (RH_{2m}), and 10-meter wind speed (V_{10m}) obtained from the WRF model with the weather station data nearest to Liège over the entire simulation period of 16 days (23rd July to 8th August 2018). Fig. 3 suggests that the model results show a good agreement with the observations. The trend of the diurnal variation of the temperature (Fig. 3(a)) and humidity (Fig. 3(b)) is captured well by the model. Furthermore, the wind velocity (Fig. 3(c)) also matches well; considering the difficulties involved in accurately modelling turbulence to predict the wind speed, the results shown in the figure satisfactorily predict the required quantities of interest.

It is important to note that, on certain days, the simulation results show a cold and wet bias during the day and night, with a higher bias at night compared to the day (in Appendix, Table A.1). The RMSE values are also lower during the day. The wind speeds follow a similar trend to the observations from the weather station with slight over and underestimations. Previous studies also report similar biases as systematic biases of the model (Lee et al., 2011; Kim et al., 2013; Giovannini et al., 2014; Jänicke et al., 2017; Wang et al., 2022; Tan et al., 2023). However, the goal of the present study is to do a comparative study of the scenarios with and without green roofs, and as such, the current predictions are indeed enough for such a study.As the simulations of all scenarios use the same physical parameterisations and configurations; they are comparable in performance and can be compared to obtain insights into scenarios with and without green roofs.

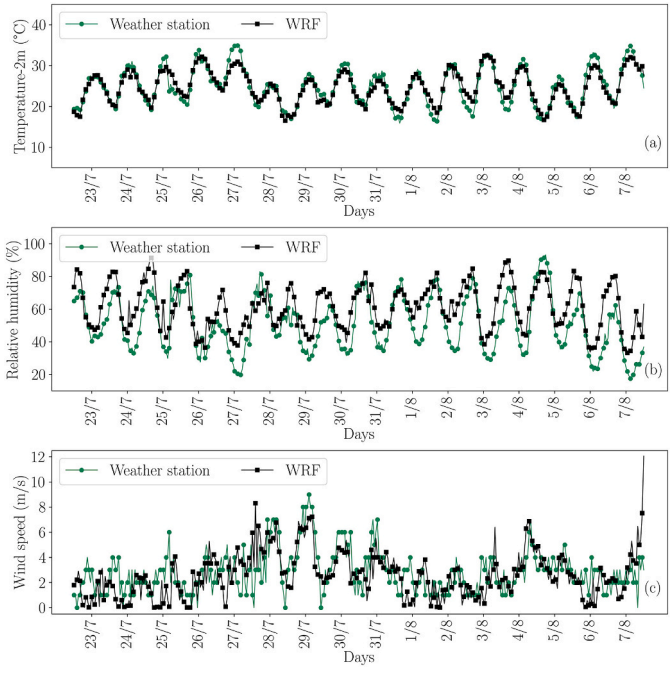

Fig. 3. Time series of (a) 2-m temperature (in °C) and (b) relative humidity (%) (c) 10-m wind speed (in ms^{-1}) for weather station (green) and output from WRF (black).

3.2. Impact of green roofs on temperature

Fig. 4(a) and (b) presents the temporal variation of differences in near-surface air temperature $(\Delta T_{air,2m})$ and surface temperature (ΔT_{se}) spatially averaged over the innermost domain for only the urban grid cells. We observe that the $\Delta T_{air,2m}$ and ΔT_{se} follow a typical diurnal cycle for each day during the entire simulation period. The $T_{air,2m}$ and T_{se} decrease during the day and slightly increase during the night. The reduction in temperatures during the day is higher in the case of an extreme scenario compared to a realistic scenario. Understandably, due to the non-linear nature of the interactions between turbulence, heat, and moisture, the reduction in temperature is not the same over all the days. Furthermore, we observe that the surface temperature has similar values over different days, however the air-temperature has more variations (Fig. 4). This can be explained by the fact that near-surface turbulence plays a major role in deciding the air temperature, which is more sensitive than the surface temperature and majorly depends on the surface energy balance caused by the radiation. While the maximum reduction in $T_{air,2m}$ is around 0.5 °C for a realistic scenario, it reduces up to 2 °C for the extreme scenario. The maximum reduction in T_{se} is around 1.5 °C in a realistic scenario, whereas it is around 4.5 °C in the extreme scenario. During the night, the increase in $T_{air,2m}$ is around 0.2 °C and 0.5 °C in extreme and realistic scenarios, respectively.

To quantify the average spatial and temporal variation of green roofs on temperature reduction, we calculate the average reduction in temperature over a 14-day period. We neglect the first two days of simulations to account for the spin-up effects. In Fig. 4 (c) and (d), we demonstrate the temporally averaged spatial variation in temperature for 24 h to examine whether the impact of green roofs varies spatially in both scenarios. While most of the $\Delta T_{air,2m}$ values are between 0.2 and 0.4 °C in a realistic scenario, the values vary between 0.75 and 1.2 °C in the extreme scenario. Similarly, in terms of T_{se}, the range of ΔT_{se} is greater for the extreme scenario compared to a realistic scenario. Most (values between 25th to 75th percentile, 50 %) of the ΔT_{se} values range from 0 to 1 °C and 1.5–3.5 °C for realistic and extreme scenarios, respectively. Spatially also, the increase in temperatures during the night in a realistic scenario is similar to the decrease in temperatures during the day.

Based on the spatial variation (in Appendix, Figs. A.2 and A.3), we observe that, on average, there is a decrease in air and surface temperature overall. This is due to the longer days during summer in Europe. We also observe that the decrease in both T_{air} and T_{se} is slightly higher on the western side of Liège (outside the city boundary) in both scenarios. In the city center, the decrease in T_{air} and T_{se} is lower.

This suggests that the T_{se} and $T_{air,2m}$ reductions are limited for a realistic scenario where a certain percentage of building roofs are greened. Moreover, in a realistic scenario, there is also warming of a similar magnitude. As the temperature changes differ spatially (in Appendix, Figs. A.2 and A.3), it may vary in different LCZs. Moreover, LCZs vary in terms of green roof potential and morphology. Therefore, in the next section, we explore the impact of realistic and extreme green roofing scenarios in each LCZ.

3.3. Green roofs and local climate zones

Fig. 5(A and B) shows the spatial variation of ΔT_{air} and ΔT_{se} for each urban LCZ within the study domain.

3.3.1. Near-surface air temperature

In the extreme scenario, during the day, the largest $\Delta T_{air,2m}$ is observed in the compact low-rise LCZ-3, followed by the open low-rise LCZ-6, compact mid-rise LCZ-2, open mid-rise LCZ-5, large low-rise LCZ-8 and sparsely built LCZ-9. Although the maximum value of $\Delta T_{air,2m}$ is observed in LCZ-6, more (around 75 %) values of $\Delta T_{air,2m}$ in LCZ-3 are greater than 1 °C, whereas only 30–50 % of the values of

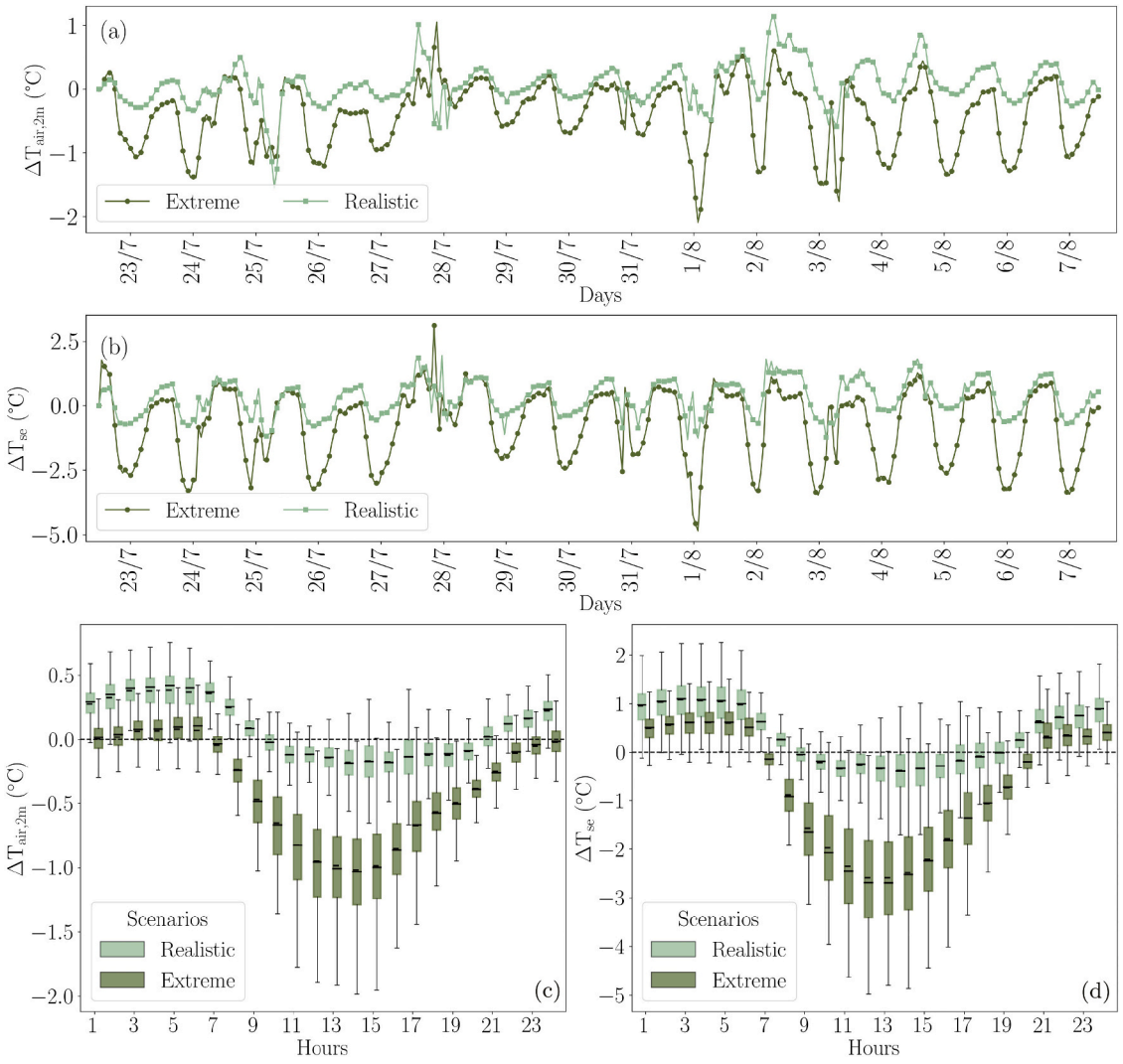

Fig. 4. Temporal variation of difference in (a) near-surface air temperature $(\Delta T_{air,2m})$ and (b) surface temperature (ΔT_{se}) in realistic and extreme scenario averaged over the innermost domain, Spatial variation of difference in (c) near-surface air temperature $(\Delta T_{air,2m})$ and (d) surface temperature (ΔT_{se}) in realistic and extreme scenario averaged over the innermost domain.

$\Delta T_{air,2m}$ are greater than 1 °C in LCZ-6. Therefore, green roofs are more effective in LCZ-3 compared to LCZ-6. The extent of reduction in $T_{air,2m}$ depends on the morphology of the LCZ. For instance, the higher $\Delta T_{air,2m}$ is observed in compact LCZs (LCZ-2 and 3) compared to open LCZs (LCZ-5 and LCZ-6, respectively). So, a larger built-up area means a higher percentage of roofs to green and a higher reduction in $T_{air,2m}$. It should be noted that low-rise LCZs perform better than high-rise LCZs in reducing air temperatures. We observe this from Fig. 5(A)(a, b, c and d), the reduction in $T_{air,2m}$ is also higher for LCZs with low-rise (LCZ-3 and 6) buildings compared to high-rise ones (LCZ-2 and 5).

Contrary to the observations in the extreme scenario, during the day, we observe the highest reduction in $T_{air,2m}$ in the large low-rise LCZ-8 in a realistic scenario. This could be due to the highest percentage of flat roofs available for greening compared to the other LCZs. This LCZ (large low-rise) is characterised by large-sized commercial or industrial buildings, which usually have large flat roofs. Compact mid-rise and low-rise, along with open mid-rise LCZs (LCZ-2,3 and 5), experience a similar range of reduction in $T_{air,2m}$, followed by open low-rise and sparsely built LCZs (LCZ-6 and 9). In a realistic scenario, we observe that building heights or density do not affect the reduction in $T_{air,2m}$. The reduction in $T_{air,2m}$ is largely dependent on the roof greening potential in each LCZ.

It is important to note that the reduction in $T_{air,2m}$ is less than 0.5 °C for most of the region within LCZ-8, with some areas experiencing a reduction in $T_{air,2m}$ of greater than 0.5 °C. Almost all the pixels of other LCZs experience a less than 0.5 °C reduction in $T_{air,2m}$. Therefore, realistic roof greening may not be beneficial in reducing the $T_{air,2m}$ in most urban areas. However, it may be beneficial in some of the areas of large low-rise LCZ-8. Moreover, there is an increase in the night-time $T_{air,2m}$ in all the LCZs.

3.3.2. *Surface temperature*

Similar to $T_{air,2m}$, in the extreme scenario, the highest reduction in T_{se} is observed in compact low-rise LCZ-3, followed by open low-rise LCZ-6, compact mid-rise LCZ-2, open mid-rise LCZ-5, large low-rise LCZ-8 and sparsely built LCZ-9. This means that greening the roofs in compact and low-rise types of LCZs can be beneficial in reducing the T_{se}. Similarly, in a realistic scenario, the highest reduction in T_{se} is observed in large low-rise LCZ-8 (similar to the trend for $\Delta T_{air,2m}$ in a realistic scenario). Almost more than 50 % of the LCZ-8 experiences a reduction of greater than 1 °C in T_{se} with realistic roof greening. Realistic roof greening in compact low-rise and open low-rise (LCZ-3 and 6), although reduces the T_{se} more than the compact and open mid-rise (LCZ-2,5), the reduction in T_{se} is less than 1 °C for most of the region in these LCZs.

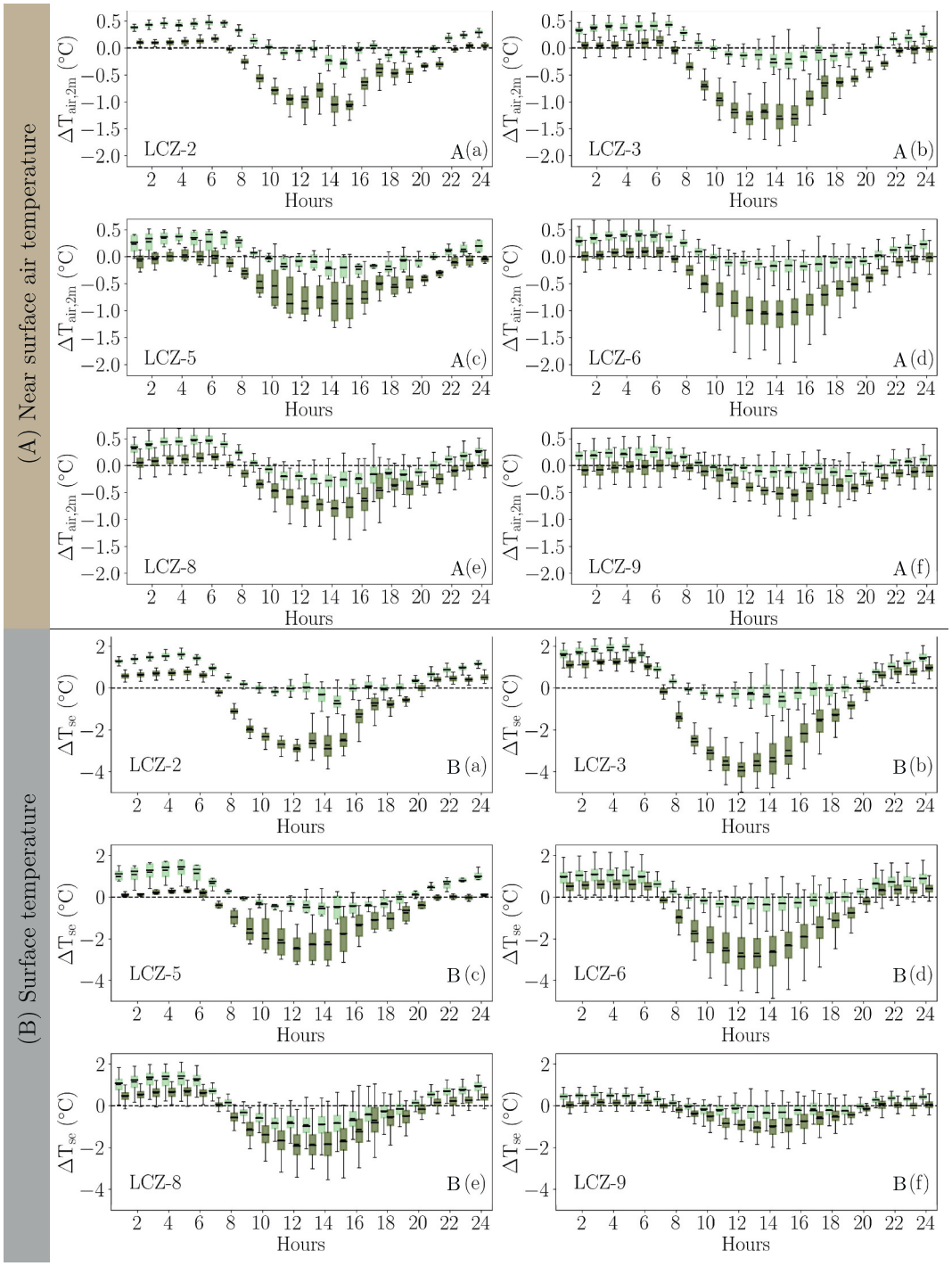

Fig. 5. Diurnal spatial variation of ΔT_{air} for A(*a*)LCZ-2, A(*b*)LCZ-3, A(*c*)LCZ-5, A(*d*)LCZ-6, A(*e*)LCZ-8, A(*f*)LCZ-9 and ΔT_{se} for B(*a*)LCZ-2, B(*b*)LCZ-3, B(*c*)LCZ-5, B(*d*) LCZ-6, B(*e*)LCZ-8, B(*f*)LCZ-9.

Therefore, realistic roof greening is not beneficial in LCZ-2,3,5 and 6. Sparsely built LCZ-9 has the lowest reduction in T_{se} because of the lowest built-up available for roof greening.

Similar to T_{air}, after introducing the green roofs, T_{se} also increases at night in all LCZs, with the same amount of increase at night as the decrease in T_{se} during the day. The increase in T_{se} at night is also higher than the decrease in T_{se} during the day for LCZ-2,3,5 and 6.

Altogether, the impact of green roofs on $T_{air,2m}$ and T_{se} in LCZs is distinctive. It depends on morphological factors such as building density and height when the percentage of roof greening is the same in all LCZs. However, when a realistic scenario is investigated, the impact of green roofs is better in large low-rise LCZ where the percentage of potential roof greening is higher. It is important to note that the reduction in temperatures in a realistic scenario is not significant in other LCZs. Moreover, night-time warming is observed in all LCZs.

3.4. Impact on UHI effect

We measure the impact of green roofs on the UHI effect using UHI intensity (UHII) during the daytime. Fig. 6 shows the air and surface UHII computed for the innermost domain. We observe that the air UHII is reduced by 1 °C and surface UHII is reduced by 3.5 °C with extreme

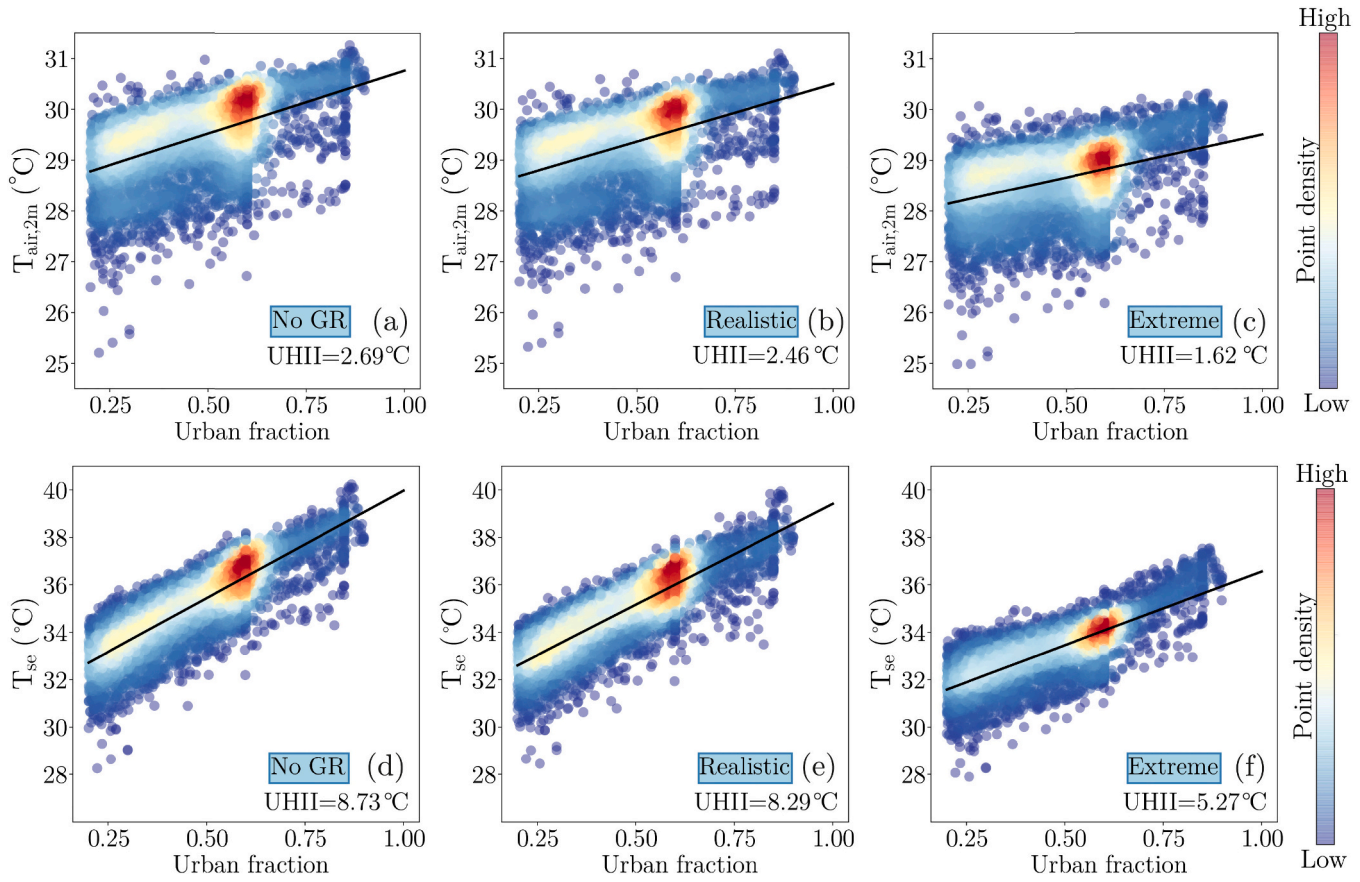

Fig. 6. Relationship between daytime T_{air} (°C) ((a), (b), (c))/daytime T_{se} (°C) ((d), (e), (f)) and the urban fraction with linear fitting (black line) for the innermost domain used for computing urban heat island intensity (UHII) in °C.

roof greening (Fig. 6(c) and (f)), whereas the air UHII is reduced by 0.25 °C and surface UHII is reduced by 0.5 °C with realistic roof greening (Fig. 6(b) and (e)). We also observe that with an increase in urban fraction, there is an increase in both T_{se} and $T_{air,2m}$, suggesting a connection between UHII and urbanisation, even in the extreme roof greening scenario. However, the increase in UHII with urbanisation is lesser with the introduction of green roofs in the study domain. The reduction in UHII is insignificant with realistic greening.

3.5. Heat index

As explained in Section 2.5.2, HI is widely used as a metric for measuring thermal comfort that includes temperature $T_{air,2m}$ and relative humidity RH. It primarily describes the perception of heat felt by a human body under a given weather, with increasing HI thermal comfort reduces. Fig. 7(a) shows the temporal variation of ΔRH (difference in RH after introducing green roofs) over the simulation period. RH increases during the day in both realistic and extreme scenarios. Looking at the spatial variation (Fig. 7(c)), we observe that the RH reduces at night for most of the region in a realistic scenario, whereas, it increases for half of the region during the night and decreases for the other half of the region in the extreme scenario. The RH increases more in the extreme scenario than in a realistic scenario during the day. The results clearly show that green roofs increase the relative humidity in extreme scenario and therefore can affect thermal comfort.

Fig. 7(b) and (d) shows the temporal and spatial variation of ΔHI (difference in HI after introducing green roofs) spatially and temporally averaged over the innermost domain urban grid cells, respectively. ΔHI follows a similar trend as observed for the $\Delta T_{air,2m}$ (Fig. 4(b) and (d)). We observe that it decreases during the day and increases during the night for both realistic and extreme scenarios. The highest reduction in HI during the day is around 1.5 °C in the extreme scenario and 0.5 °C in a realistic scenario. On average, the reduction in HI is 0.2 °C and 0.8 °C for realistic and extreme scenarios, respectively. We observe that the difference in terms of $T_{air,2m}$ (2 °C - maximum during the day) is higher than the difference obtained in terms of HI (1.5 °C - maximum during the day). This shows that the HI value has included the effects of RH in the calculation, which is important for thermal comfort.

As mentioned previously, an increase in RH at a constant temperature reduces thermal comfort. However, in our simulations, though the RH has increased during the day for the extreme scenario, there is a correspondingly larger reduction in $T_{air,2m}$, which causes a net reduction in the HI in the extreme scenario. On the other hand, in the realistic scenario, some of the pixels (the values greater than 75th percentile of ΔHI in the day-time box plots for a realistic scenario) experience an increase in HI ($\Delta HI > 0$) during the day (Fig. 7(d)). This could be due to an increase in $T_{air,2m}$ in some parts of the region (Fig. 4(c)). Since the $T_{air,2m}$ increases during the night, the HI also increases during the night. Moreover, in a realistic scenario, the increase in HI during the night is more than the decrease observed during the day. Therefore, realistic roof greening has limited benefits even in terms of thermal comfort.

3.6. Impacts on boundary layer

To further understand the effect of realistic and extreme green roofing scenarios on UHI, we investigate their impact on the boundary layer. For this, we show the time series of differences in vertical profiles (2 km above ground level (AGL)) of T_{air}, RH, wind speed (V) and turbulent kinetic energy (TKE) for both realistic and extreme scenarios. We observe a reduction in T_{air} almost every day between 0.5 and 1.5 km.

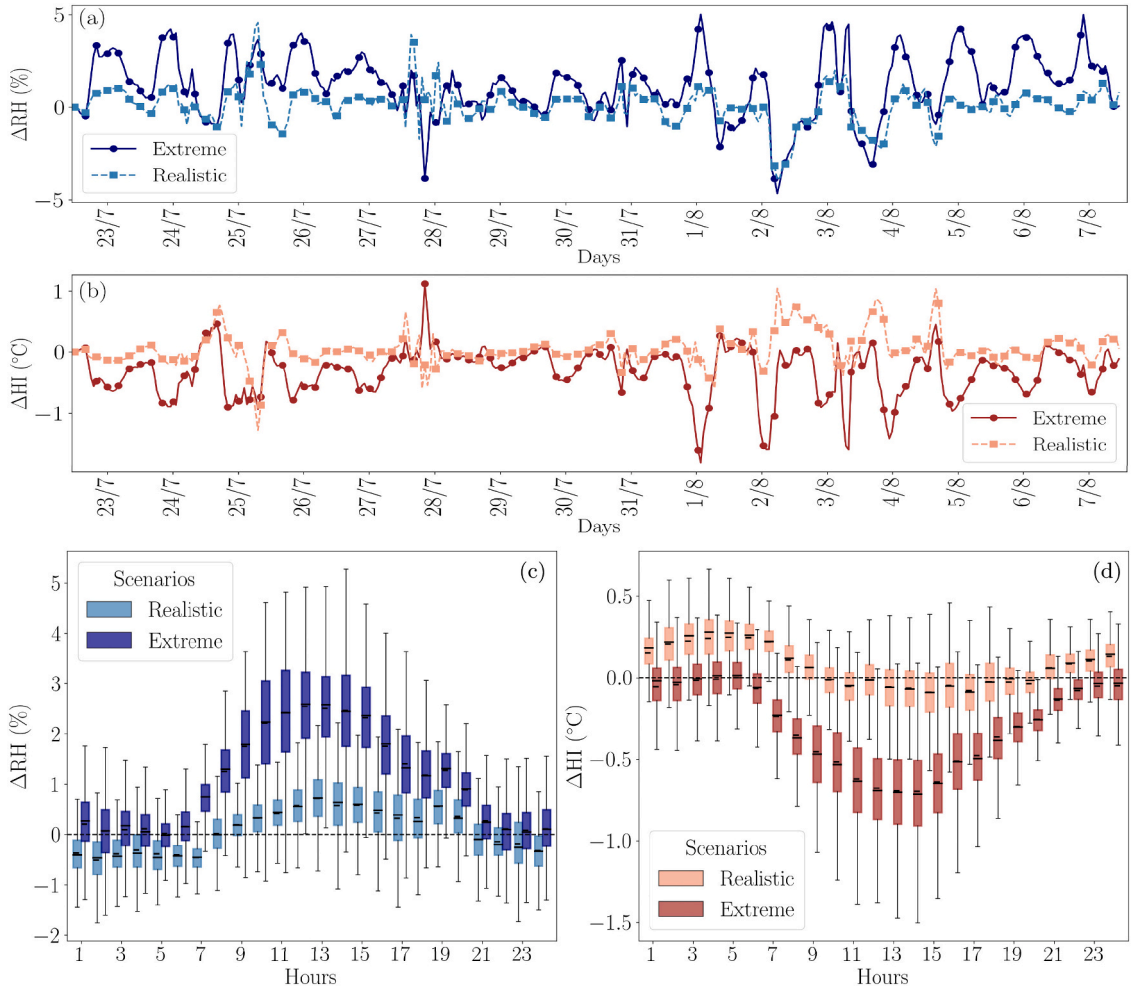

Fig. 7. Temporal variation (spatially averaged for each hour) of differences in (a) relative humidity and (b) heat index for realistic and extreme scenarios, spatial variation (temporally averaged for each hour) of differences in (c) relative humidity and (d) heat index for realistic and extreme scenarios.

The reduction is also observed below 0.5 km during the day, but there is an increase in the night (Fig. 8(a) and (b)). The T_{air} reduction is higher in the extreme greening scenario compared to a realistic scenario. While the reduction in T_{air} is less than 0.5 °C in a realistic scenario, the reduction in T_{air} is nearly zero on 27th July (highest daily temperature) in a realistic scenario. Additionally, the increase in T_{air} near the surface during the night time is around 0.5–1.5 °C in a realistic scenario for almost all days. The increase in T_{air} during the night near the surface is also observed in the extreme scenarios for a few days but is less than 1 °C. Moreover, the reduction in T_{air} in the extreme scenario is much higher compared to a realistic scenario between 0.5 and 1.5 km height.

Over most of the days during the warm afternoon, we observe a decrease in horizontal wind speed (Fig. 8(c) and (d)) near the surface (<0.5 km) because of the reduced vertical mixing (Fig. 8(e) and (f)) due to a reduction in T_{air}. A decrease in the temperature increases the stability of the boundary layer, which in turn causes a reduction in the TKE (Gadde et al., 2021), causing a reduced vertical mixing. The reduced vertical mixing near the surface led to stronger airflow over the higher levels with a reduction in momentum shift from higher to lower levels. This reduces the wind speeds near the surface generating stronger (weaker) wind speeds at higher (lower) levels.

Delving into the vertical profile of ΔRH (Fig. 8(g) and (h)), we observe that the RH increases with retrofitting green roofs for most of the vertical profile. However, the increase is lower in a realistic scenario compared to the extreme scenario. This increase can be attributed to the higher evapotranspiration with roof greening and lower wind speeds. Largely, since the T_{air} is not reduced significantly and also increases during the night, with a slight rise in RH, the heatwave is not mitigated but the effects are worsened in a realistic scenario near the surface. For the same time period, however, the extreme scenario has reduced T_{air} but increased RH. This scenario could be beneficial to reduce the T_{air}, but may exacerbate the RH in the region. It is important to note that the increase in RH here is without irrigation on the green roofs. With irrigation, the T_{air} may be reduced but the RH may increase even more.

Studies indicate that implementing green roofs at a large scale can lead to an increase in relative humidity in urban areas (Li et al., 2014; Sharma et al., 2016; Zonato et al., 2021; Georgescu et al., 2014). This is attributed to changes in vertical mixing and evapotranspiration caused by green roofs. Specifically, the decrease in sensible heat flux with green roofs stabilises the atmosphere (lower TKE as seen in Fig. 8(e) and (f)) and reduces vertical mixing over cities (Yang et al., 2016). Consequently, the internal boundary layer expands more slowly, diminishing the influence of urban surface conditions on the atmosphere and increasing the impact of upwind surfaces (Li et al., 2014; Sharma et al., 2016). This can result in the advection of moist air from rural to urban areas, thereby elevating relative humidity in urban regions Li et al. (2014).

4. Conclusions

In this study, we evaluate the impact of a realistic fraction of green roofs in each LCZ class on the UHI effect during a heatwave in Liège City,

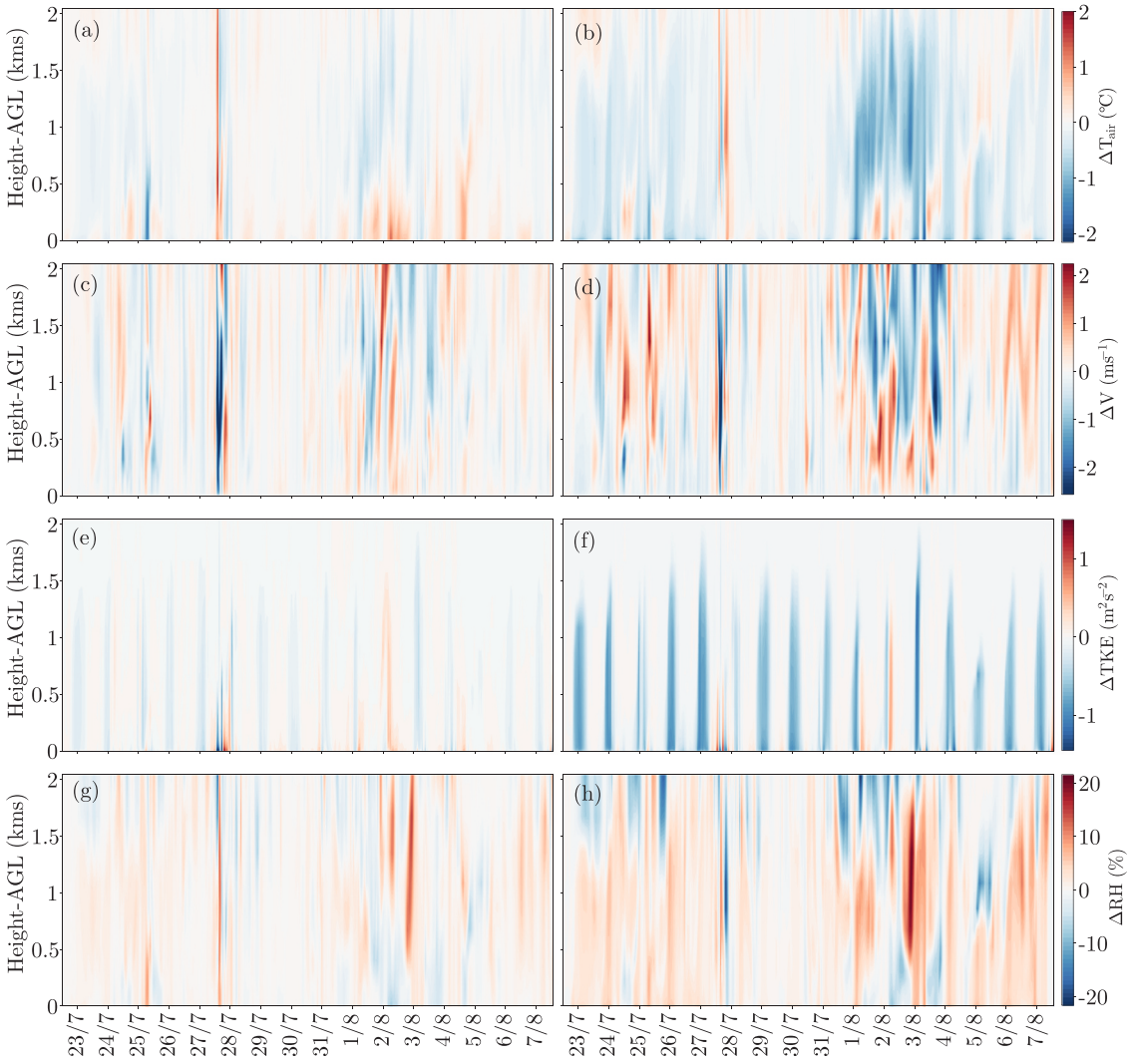

Fig. 8. Vertical profile of differences in air temperature, wind speed, turbulent kinetic energy and relative humidity for realistic ((a), (c), (e), (g)) and extreme ((b), (d), (f), (h)) scenarios with spatially averaged values for urban innermost domain from July 23–August 7, 2018.

employing a high-resolution WRF study using the BEP-BEM parameterisation with LCZ land use classification. We ran the WRF simulation for a base scenario (without green roofs), a realistic scenario (green roof fraction derived from remote sensing) and an extreme scenario for the longest and most severe heatwave in Liège from 23rd July to 8th August 2018. We observe a reduction in near-surface air and surface temperatures after introducing green roofs in the study domain. Our results concerning air and surface temperature changes after introducing green roofs in the extreme scenario align with other green roof studies (Tan et al., 2023; Sharma et al., 2016; Georgescu et al., 2014). These studies also suggest nighttime warming due to green roofs, mainly because of the accumulation of extra solar radiation during the daytime by rooftop soil layers discharged at night (Sharma et al., 2016; Georgescu et al., 2014).

Comparing realistic and extreme scenarios, we observe that realistic roof greening has a much less significant effect on reducing the near-surface air temperature (0.5 °C maximum) and surface temperature (1.5 °C maximum) throughout the simulation period than the extreme scenario. However, it is important to note that the green roof modelled in this study has a specific set of properties (albedo, emissivity, LAI and irrigation). Studies (Saadatian et al., 2013; Jamei et al., 2021) have demonstrated that green roofs with higher LAI can more efficiently reduce near-surface temperatures. Moreover, previous studies suggest that irrigation significantly improves the performance of green roofs in reducing the temperatures (Heusinger et al., 2018; MacIvor et al., 2016; Wang et al., 2022; Tewari et al., 2019). In this work, the green roofs were modelled with no irrigation, which could have reduced their potential to mitigate UHI. Nevertheless, deploying irrigated green roofs increases the installation and maintenance costs and due to structural considerations, the potential roofs for greening existing buildings would be further reduced. Future studies should conduct a sensitivity analysis of green roof parameters to identify optimal green roofs and analyse their impact at a regional scale with realistic fractions.

Further investigating the impact of green roofs in each LCZ in Liège, we observe that the decrease in air and surface temperature depends on the urban morphology when the green roof fraction is the same for all LCZs. For instance, the temperature decrease is higher in compact, low-rise, and highly dense LCZs when all the roofs are green. This result is similar to the idealised two-dimensional experiments by Zonato et al. (2021), which suggest that the mitigation effect from green roofs on air temperature varies linearly with building density during summer. Other studies also report that the mitigation effect of green roofs is higher for low-rise buildings (Berardi et al., 2014; Iaria and Susca, 2022; Susca, 2019). In realistic roof greening, the magnitude of the effect is mainly dependent on the green roof fraction. Therefore, the large low-rise LCZ (LCZ-8) characterised by large industrial or commercial buildings in Liège City has a higher temperature reduction than other LCZs. It is important to know that the decrease in temperature in LCZ-8 is also

limited in a realistic scenario.

Since the green roofs reduce the temperatures during the day, we also investigate the reduction in UHI intensity (UHII) during the day. We observe that the air and surface UHII are reduced by deploying green roofs. The reduction is higher with extreme roof greening compared to a realistic one, with minimal reduction in a realistic scenario. Another thing to note is that, even in both green roof scenarios, the air and surface temperatures increase with the increase in urban fraction. Tan et al. (2023) reports a similar result regarding green roofs and suggests that deploying cool roofs can be better since the temperature is lower with an increase in urban fraction.

As human thermal comfort is also an indicator of the UHI effect along with temperatures, we calculated the heat index, which relates to air temperature and relative humidity. We observed that green roofs reduce the heat index. Green roofs increase the relative humidity during the day because of the evapotranspiration. Nevertheless, since the reduction in temperature is higher, the heat index is reduced even with a higher increase in relative humidity in the extreme scenario. In the extreme scenario, the nighttime heat index is also not increased for half of the region, suggesting the effectiveness of green roofs. In a realistic scenario, however, the heat index does not reduce as much as it increases at night. So, realistic roof greening worsens the heat index for most parts of the city at night. Additionally, after looking at the vertical profiles of relative humidity, air temperature and wind speeds, we notice that green roofs may exacerbate the relative humidity in the urban area.

Altogether, we conclude that realistic roof greening across the LCZs in Liège may not be sufficient to reduce the UHI effect at a city scale. While green roof deployment is beneficial in mitigating UHI at the rooftop level in block/neighbourhood scale studies (Susca, 2019), their impact on reducing the UHI is insignificant at the city scale. Our study shows the importance of considering realistic green roof fractions in analysing their impact on the UHI effect. This study can be further refined by incorporating the spatial variation of potential green roof fraction, which varies for each pixel. Further studies should explore the coupling of green roofs with other mitigation strategies for city-wide implementation and impact. In this study, for Liège, we consider all the flat roofs as the roofs that can be greened. However, the realistic potential will be even less with structural constraints, especially in European cities with sloped roofed buildings. This research provides valuable insights for policymakers implementing green roofs on a city-wide scale. Furthermore, as our study reports spatial, temporal and typological variability of the impact of green roofs on the UHI effect, it delivers a comprehensive overview of the impacts.

CRediT authorship contribution statement

Mitali Yeshwant Joshi: Writing – original draft, Software, Methodology, Formal analysis, Data curation, Conceptualization. **Jacques Teller:** Writing – review & editing, Supervision, Methodology, Funding acquisition, Conceptualization.

Declaration of competing interest

The authors declare that they have no known competing financial interests or personal relationships that could have appeared to influence the work reported in this paper.

Data availability

Data will be made available on request.

Acknowledgments

Computational resources for this study have been provided by the Consortium des Équipements de Calcul Intensif (CÉCI), funded by the Fonds de la Recherche Scientifique de Belgique (F.R.S.-FNRS) under Grant No. 2.5020.11 and by the Walloon Region. We would also like to thank Dr. Srinidhi Gadde from University of Twente for the technical help to run WRF model on CÉCI cluster.

Funding

This research was funded through the ARC grant for Concerted Research Actions for project number 19/23–28 "CityRoof" financed by the French Community of Belgium (Wallonia-Brussels Federation).

Appendix A

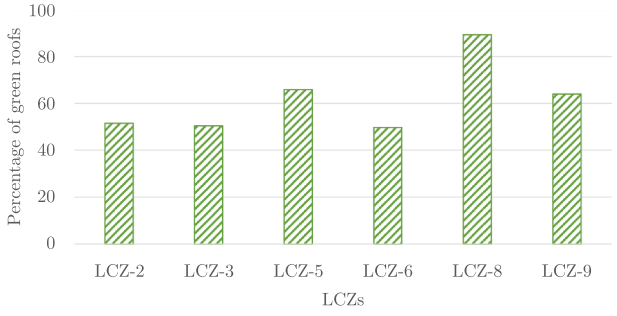

Fig. A.1. Percentage of green roofs.

Table A.1
Summary of mean absolute error (MAE) and root mean squared error (RMSE) for simulated and weather station data of $T_{air,2m}$, RH_{2m}, and V_{10m} during day (04:00–18:00) and night (19:00–4:00) for entire simulation.

	MAE			RMSE		
	Day	Night	Total	Day	Night	Total
$T_{air,2m}$	−0.08	−0.17	−0.167	0.741	1.6865	1.659

(*continued on next page*)

Table A.1 (*continued*)

	MAE			RMSE		
	Day	Night	Total	Day	Night	Total
V_{10m}	−1.29	−0.20	−0.244	1.88	1.72	1.731
RH_{2m}	4.13	10.14	9.91	7.23	14.46	14.25

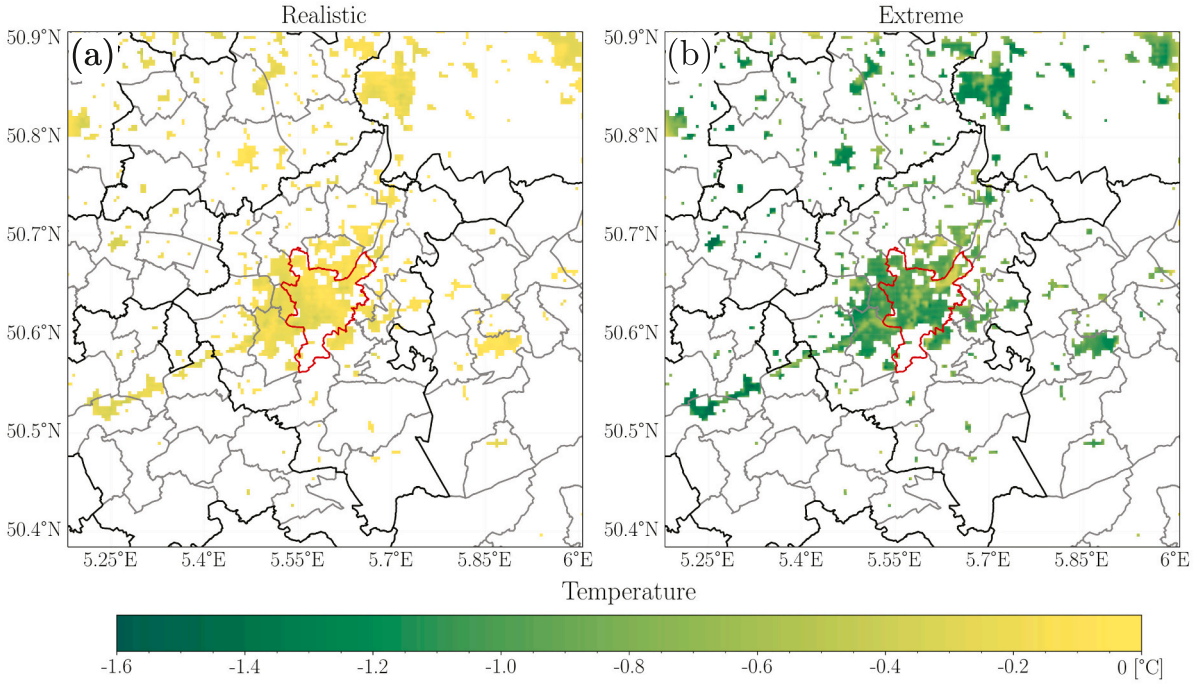

Fig. A.2. Spatial variation of temporally averaged differences in air temperatures (a) realistic scenario (b) extreme scenario.

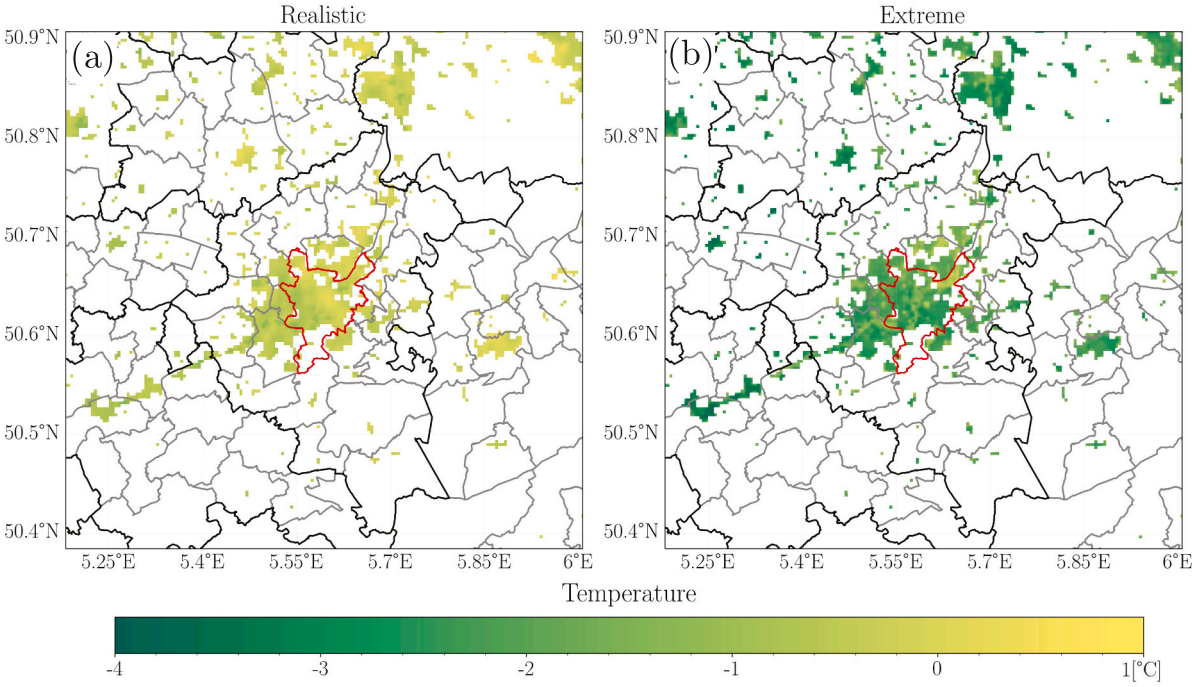

Fig. A.3. Spatial variation of temporally averaged differences in surface temperatures (a) realistic scenario (b) extreme scenario.

References

Berardi, U., GhaffarianHoseini, A., GhaffarianHoseini, A., 2014. State-of-the-art analysis of the environmental benefits of green roofs. Appl. Energy 115, 411–428.

Blackhurst, M., Hendrickson, C., Matthews, H.S., 2010. Cost-effectiveness of green roofs. J. Archit. Eng. 16 (4), 136–143.

Bougeault, P., Lacarrere, P., 1989. Parameterization of orography-induced turbulence in a mesobeta–scale model. Mon. Weather Rev. 117 (8), 1872–1890.

Bou-Zeid, E., Parlange, M.B., Meneveau, C., 2007. On the parameterization of surface roughness at regional scales. J. Atmos. Sci. 64 (1), 216–227.

Broadbent, A.M., Krayenhoff, E.S., Georgescu, M., 2020. Efficacy of cool roofs at reducing pedestrian-level air temperature during projected 21st century heatwaves in Atlanta, Detroit, and Phoenix (USA). Environ. Res. Lett. 15 (8), 084007.

Brousse, O., Martilli, A., Foley, M., Mills, G., Bechtel, B., 2016. Wudapt, an efficient land use producing data tool for mesoscale models? Integration of urban lcz in wrf over Madrid. Urban Clim. 17, 116–134.

Castleton, H.F., Stovin, V., Beck, S.B., Davison, J.B., 2010. Green roofs; building energy savings and the potential for retrofit. Energy Build. 42 (10), 1582–1591.

Chen, F., Dudhia, J., 2001. Coupling an advanced land surface–hydrology model with the Penn State–ncar mm5 modeling system. Part i: model implementation and sensitivity. Mon. Weather Rev. 129 (4), 569–585.

Chen, K., Newman, A.J., Huang, M., Coon, C., Darrow, L.A., Strickland, M.J., Holmes, H. A., 2022. Estimating heat-related exposures and urban heat island impacts: a case study for the 2012 Chicago heatwave. GeoHealth 6 (1), e2021GH000535.

Chew, L.W., Liu, X., Li, X.-X., Norford, L.K., 2021. Interaction between heat wave and urban heat island: a case study in a tropical coastal city, Singapore. Atmos. Res. 247, 105134.

Da Silva, J., Vicente, R., 2013. Pathology and defects of building façades and roofs: a state-of-the-art report on building pathology. In: Building Pathology, pp. 123–131.

de Munck, C., Pigeon, G., Masson, V., Meunier, F., Bousquet, P., Tréméac, B., Merchat, M., Poeuf, P., Marchadier, C., 2013. How much can air conditioning increase air temperatures for a city like Paris, France? Int. J. Climatol. 33 (1), 210–227.

Demuzere, M., Bechtel, B., Middel, A., Mills, G., 2019a. European LCZ Map (version2). figshare.

Demuzere, M., Bechtel, B., Middel, A., Mills, G., 2019b. Mapping europe into local climate zones. PLoS One 14 (4), e0214474.

Demuzere, M., Argüeso, D., Zonato, A., Kittner, J., 2022. W2W: a Python package that injects WUDAPT's local climate zone information in WRF. J. Open Source Soft. 7 (76), 4432.

Doutreloup, S., Fettweis, X., Rahif, R., Elnagar, E., Pourkiaei, M.S., Amaripadath, D., Attia, S., 2022. Historical and future weather data for dynamic building simulations in Belgium using the regional climate model mar: typical and extreme meteorological year and heatwaves. Earth Syst. Sci. Data 14 (7), 3039–3051.

Ek, M., Mitchell, K., Lin, Y., Rogers, E., Grunmann, P., Koren, V., Gayno, G., Tarpley, J., 2003. Implementation of noah land surface model advances in the national centers for environmental prediction operational mesoscale eta model. J. Geophys. Res. Atmos. 108 (D22).

Ferreira, C., Silva, A., Brito, J.d., S. Dias, I., Flores-Colen, I., 2020. Maintenance modelling of ceramic claddings in pitched roofs based on the evaluation of their in situ degradation condition. Infrastructures 5 (9), 77.

Gabriel, K.M., Endlicher, W.R., 2011. Urban and rural mortality rates during heat waves in Berlin and Brandenburg, Germany. Environ. Pollut. 159 (8), 2044–2050 (Selected papers from the conference Urban Environmental Pollution: Overcoming Obstacles to Sustainability and Quality of Life (UEP2010), 20-23 June 2010, Boston, USA).

Gadde, S.N., Stieren, A., Stevens, R.J., 2021. Large-Eddy simulations of stratified atmospheric boundary layers: comparison of different subgrid models. Bound.-Layer Meteorol. 178 (3), 363–382.

Georgescu, M., Morefield, P.E., Bierwagen, B.G., Weaver, C.P., 2014. Urban adaptation can roll back warming of emerging megapolitan regions. Proc. Natl. Acad. Sci. 111 (8), 2909–2914.

Gilabert, J., Ventura, S., Segura, R., Martilli, A., Badia, A., Llasat, C., Corbera, J., Villalba, G., 2021. Abating heat waves in a coastal mediterranean city: what can cool roofs and vegetation contribute? Urban Clim. 37, 100863.

Giovannini, L., Zardi, D., De Franceschi, M., Chen, F., 2014. Numerical simulations of boundary-layer processes and urban-induced alterations in an alpine valley. Int. J. Climatol. 34 (4), 1111–1131.

Grunwald, L., Heusinger, J., Weber, S., 2017. A gis-based mapping methodology of urban green roof ecosystem services applied to a central European city. Urban For. Urban Green. 22, 54–63.

Gunawardena, K., Wells, M., Kershaw, T., 2017. Utilising green and bluespace to mitigate urban heat island intensity. Sci. Total Environ. 584-585, 1040–1055 (Cited by: 526; All Open Access, Green Open Access, Hybrid Gold Open Access).

Gutierrez, E., 2016. Quantification of Environmental Impacts of Heat Fluxes From Built Environments. PhD thesis. The City College of New York.

Hammerberg, K., Brousse, O., Martilli, A., Mahdavi, A., 2018. Implications of employing detailed urban canopy parameters for mesoscale climate modelling: a comparison between wudapt and gis databases over Vienna, Austria. Int. J. Climatol. 38, e1241–e1257.

He, C., He, L., Zhang, Y., Kinney, P.L., Ma, W., 2020. Potential impacts of cool and green roofs on temperature-related mortality in the Greater Boston Region. Environ. Res. Lett. 15 (9), 094042.

Hersbach, H., Bell, B., Berrisford, P., Hirahara, S., Horányi, A., Muñoz-Sabater, J., Nicolas, J., Peubey, C., Radu, R., Schepers, D., et al., 2020. The era5 global reanalysis. Q. J. R. Meteorol. Soc. 146 (730), 1999–2049.

Heusinger, J., Sailor, D.J., Weber, S., 2018. Modeling the reduction of urban excess heat by green roofs with respect to different irrigation scenarios. Build. Environ. 131, 174–183.

Iacono, M.J., Delamere, J.S., Mlawer, E.J., Shephard, M.W., Clough, S.A., Collins, W.D., 2008. Radiative forcing by long-lived greenhouse gases: calculations with the aer radiative transfer models. J. Geophys. Res. Atmos. 113 (D13).

Iaria, J., Susca, T., 2022. Analytic hierarchy processes (AHP) evaluation of green roof- and green wall-based UHI mitigation strategies via ENVI-met simulations. Urban Clim. 46, 101293.

Jacob, D., Petersen, J., Eggert, B., Alias, A., Bøssing Christensen, O., Bouwer, L., Braun, A., Colette, A., Déqué, M., Georgievski, G., et al., 2013. Eurocordex: new high-resolution climate change projections for european impact research. Reg. Environ. Chang. 14, 563–578.

Jamei, E., Chau, H.W., Seyedmahmoudian, M., Stojcevski, A., 2021. Review on the cooling potential of green roofs in different climates. Sci. Total Environ. 791, 148407.

Jänicke, B., Meier, F., Fenner, D., Fehrenbach, U., Holtmann, A., Scherer, D., 2017. Urban–rural differences in near-surface air temperature as resolved by the Central Europe Refined analysis (CER): sensitivity to planetary boundary layer schemes and urban canopy models. Int. J. Climatol. 37 (4), 2063–2079.

Janjic, Z., 2002. Nonsingular implementation of the Mellor-Yamada level 2.5 scheme in the NCEP meso model, NCEP Off. Note 437, 61.

Joshi, M.Y., Teller, J., 2021. Urban integration of green roofs: current challenges and perspectives. Sustainability 13 (22), 12378.

Joshi, M., Selmi, W., Binard, M., Nys, G.-A., Teller, J., 2020. Potential for urban greening with green roofs: a way towards smart cities. ISPRS Ann. Photogramm. Remote Sens. Spat. Inf. Sci. 6, 87–94.

Joshi, M., Amaripadath, D., Machard, A., Attia, S., 2022. Heatwaves Identification Classification and Visualisation With Python.

Kalogeri, C., Spyrou, C., Koukoula, M., Saviolakis, P.M., Pappa, A., Loupis, M., Masouras, C., Katsafados, P., 2023. Modeling the impact of the green roofs as a nature-based solution to mitigate the urban heat island effects over Attica, Greece. Environ. Sci. Proc. 26 (1), 174.

Karteris, M., Theodoridou, I., Mallinis, G., Tsiros, E., Karteris, A., 2016. Towards a green sustainable strategy for mediterranean cities: assessing the benefits of large-scale green roofs implementation in Thessaloniki, northern Greece, using environmental modelling, gis and very high spatial resolution remote sensing data. Renew. Sust. Energ. Rev. 58, 510–525.

Kim, Y., Sartelet, K., Raut, J.-C., Chazette, P., 2013. Evaluation of the weather research and forecast/urban model over Greater Paris. Bound.-Layer Meteorol. 149, 105–132.

Kumar, A., Chen, F., Barlage, M., Ek, M.B., Niyogi, D., 2014. Assessing impacts of integrating modis vegetation data in the weather research and forecasting (WRF) model coupled to two different canopy-resistance approaches. J. Appl. Meteorol. Climatol. 53 (6), 1362–1380.

Lee, S.-H., Kim, S.-W., Angevine, W., Bianco, L., McKeen, S., Senff, C., Trainer, M., Tucker, S., Zamora, R., 2011. Evaluation of urban surface parameterizations in the wrf model using measurements during the Texas air quality study 2006 field campaign. Atmos. Chem. Phys. 11 (5), 2127–2143.

Li, D., Bou-Zeid, E., 2013. Synergistic interactions between urban heat islands and heat waves: the impact in cities is larger than the sum of its parts. J. Appl. Meteorol. Climatol. 52 (9), 2051–2064 (Cited by: 535; All Open Access, Bronze Open Access).

Li, X.-X., Liu, X., 2021. Effect of tree evapotranspiration and hydrological processes on urban microclimate in a tropical city: a WRF/SLUCM study. Urban Clim. 40, 101009.

Li, X.-X., Norford, L.K., 2016. Evaluation of cool roof and vegetations in mitigating urban heat island in a tropical city, Singapore. Urban Clim. 16, 59–74.

Li, D., Bou-Zeid, E., Oppenheimer, M., 2014. The effectiveness of cool and green roofs as urban heat island mitigation strategies. Environ. Res. Lett. 9, 055002.

Li, D., Sun, T., Liu, M., Yang, L., Wang, L., Gao, Z., 2015. Contrasting responses of urban and rural surface energy budgets to heat waves explain synergies between urban heat islands and heat waves. Environ. Res. Lett. 10 (5) (Cited by: 150; All Open Access, Gold Open Access, Green Open Access).

Li, D., Sun, T., Liu, M., Wang, L., Gao, Z., 2016. Changes in wind speed under heat waves enhance urban heat islands in the Beijing metropolitan area. J. Appl. Meteorol. Climatol. 55 (11), 2369–2375 (Cited by: 52; All Open Access, Bronze Open Access, Green Open Access).

Li, H., Zhou, Y., Wang, X., Zhou, X., Zhang, H., Sodoudi, S., 2019. Quantifying urban heat island intensity and its physical mechanism using WRF/UCM. Sci. Total Environ. 650, 3110–3119.

Liao, W., Liu, X., Li, D., Luo, M., Wang, D., Wang, S., Baldwin, J., Lin, L., Li, X., Feng, K., et al., 2018. Stronger contributions of urbanization to heat wave trends in wet climates. Geophys. Res. Lett. 45 (20), 11–310.

Liu, N., Morawska, L., 2020. Modeling the urban heat island mitigation effect of cool coatings in realistic urban morphology. J. Clean. Prod. 264, 121560.

Liu, X., Tian, G., Feng, J., Hou, H., Ma, B., 2022. Adaptation strategies for urban warming: assessing the impacts of heat waves on cooling capabilities in Chongqing, China. Urban Clim. 45, 101269.

Lu, H., Gaur, A., Krayenhoff, E.S., Jandaghian, Z., Lacasse, M., Moore, T., 2023. Thermal effects of cool roofs and urban vegetation during extreme heat events in three Canadian regions. Sustain. Cities Soc. 99, 104925.

Machard, A., 2022. Amachard/assembling-future-weather-files-including-heatwaves: V1. 0.0.

MacIvor, J.S., Margolis, L., Perotto, M., Drake, J.A., 2016. Air temperature cooling by extensive green roofs in Toronto Canada. Ecol. Eng. 95, 36–42.

Martilli, A., Brousse, O., Ching, J., 2016. Urbanized WRF modeling using WUDAPT. In: Technical Report March. Cientro de Investigaciones Energeticas MedioAmbientales y Tecnologicas (CIEMAT).

Marvuglia, A., Koppelaar, R., Rugani, B., 2020. The effect of green roofs on the reduction of mortality due to heatwaves: results from the application of a spatial microsimulation model to four european cities. Ecol. Model. 438, 109351.
McRae, I., Freedman, F., Rivera, A., Li, X., Dou, J., Cruz, I., Ren, C., Dronova, I., Fraker, H., Bornstein, R., 2020. Integration of the WUDAPT, WRF, and ENVI-met models to simulate extreme daytime temperature mitigation strategies in San Jose, California. Build. Environ. 184, 107180.
Meijer, F., Itard, L., Sunikka-Blank, M., 2009. Comparing european residential building stocks: performance, renovation and policy opportunities. Build. Res. Inf. 37 (5–6), 533–551.
Mohan, M., Gupta, A., Bhati, S., 2013. A modified approach to analyze thermal comfort classification. Atmos. Clim. Sci. 2014.
Morini, E., Touchaei, A.G., Rossi, F., Cotana, F., Akbari, H., 2018. Evaluation of albedo enhancement to mitigate impacts of urban heat island in Rome (Italy) using wrf meteorological model. Urban Clim. 24, 551–566.
Mughal, M., Li, X.-X., Norford, L.K., 2020. Urban heat island mitigation in Singapore: evaluation using wrf/multilayer urban canopy model and local climate zones. Urban Clim. 34, 100714.
Ouzeau, G., Soubeyroux, J.-M., Schneider, M., Vautard, R., Planton, S., 2016. Heat waves analysis over France in present and future climate: application of a new method on the euro-cordex ensemble. Clim. Serv. 4, 1–12.
Patel, P., Karmakar, S., Ghosh, S., Niyogi, D., 2020. Improved simulation of very heavy rainfall events by incorporating wudapt urban land use/land cover in WRF. Urban Clim. 32, 100616.
Patz, J.A., Campbell-Lendrum, D., Holloway, T., Foley, J.A., 2005. Impact of regional climate change on human health. Nature 438, 310–317, 2005 438:7066.
Ribeiro, I., Martilli, A., Falls, M., Zonato, A., Villalba, G., 2021. Highly resolved WRF-BEP/BEM simulations over Barcelona urban area with LCZ. Atmos. Res. 248, 105220.
Rothfusz, L.P., Headquarters, N.S.R., 1990. The Heat Index Equation (or, More Than You Ever Wanted to Know About Heat Index), 9023. National Oceanic and Atmospheric Administration, National Weather Service, Office of Meteorology, Fort Worth, Texas, p. 640.
Saadatian, O., Sopian, K., Salleh, E., Lim, C., Riffat, S., Saadatian, E., Toudeshki, A., Sulaiman, M., 2013. A review of energy aspects of green roofs. Renew. Sust. Energ. Rev. 23, 155–168.
Salamanca, F., Martilli, A., 2010. A new building energy model coupled with an urban canopy parameterization for urban climate simulations—part II. Validation with one dimension off-line simulations. Theor. Appl. Climatol. 99, 345–356.
Santamouris, M., Synnefa, A., Karlessi, T., 2011. Using advanced cool materials in the urban built environment to mitigate heat islands and improve thermal comfort conditions. Sol. Energy 85 (12), 3085–3102 (Cited by: 665).
Santamouris, M., Haddad, S., Saliari, M., Vasilakopoulou, K., Synnefa, A., Paolini, R., Ulpiani, G., Garshasbi, S., Fiorito, F., 2018. On the energy impact of urban heat island in Sydney: climate and energy potential of mitigation technologies. Energy Build. 166, 154–164.
Santos, T., Tenedório, J.A., Gonçalves, J.A., 2016. Quantifying the city's green area potential gain using remote sensing data. Sustainability 8 (12), 1247.
Segura, R., Badia, A., Ventura, S., Gilabert, J., Martilli, A., Villalba, G., 2021. Sensitivity study of pbl schemes and soil initialization using the WRF-BEP-BEM model over a mediterranean coastal city. Urban Clim. 39, 100982.
Sharma, A., Conry, P., Fernando, H.J.S., Hamlet, A.F., Hellmann, J.J., Chen, F., 2016. Green and cool roofs to mitigate urban heat island effects in the Chicago metropolitan area: evaluation with a regional climate model. Environ. Res. Lett. 11 (6), 064004.
Steadman, R.G., 1979. The assessment of sultriness. Part I: a temperature-humidity index based on human physiology and clothing science. J. Appl. Meteorol. Climatol. 18 (7), 861–873.
Stewart, I.D., Oke, T.R., 2012. Local climate zones for urban temperature studies. Bull. Am. Meteorol. Soc. 93 (12), 1879–1900.
Sun, T., Grimmond, C., Ni, G.-H., 2016. How do green roofs mitigate urban thermal stress under heat waves? J. Geophys. Res. Atmos. 121 (10), 5320–5335.
Susca, T., 2019. Green roofs to reduce building energy use? A review on key structural factors of green roofs and their effects on urban climate. Build. Environ. 162, 106273.
Synnefa, A., Dandou, A., Santamouris, M., Tombrou, M., Soulakellis, N., 2008. On the use of cool materials as a heat island mitigation strategy. J. Appl. Meteorol. Climatol. 47 (11), 2846–2856.
Tan, H., Kotamarthi, R., Wang, J., Qian, Y., Chakraborty, T., 2023. Impact of different roofing mitigation strategies on near-surface temperature and energy consumption over the Chicago metropolitan area during a heatwave event. Sci. Total Environ. 860, 160508.
Tewari, M., Yang, J., Kusaka, H., Salamanca, F., Watson, C., Treinish, L., 2019. Interaction of urban heat islands and heat waves under current and future climate conditions and their mitigation using green and cool roofs in New York city and Phoenix, Arizona. Environ. Res. Lett. 14 (3), 034002.
Thompson, G., Eidhammer, T., 2014. A study of aerosol impacts on clouds and precipitation development in a large winter cyclone. J. Atmos. Sci. 71 (10), 3636–3658.
Wang, X., Li, H., Sodoudi, S., 2022. The effectiveness of cool and green roofs in mitigating urban heat island and improving human thermal comfort. Build. Environ. 217, 109082.
Yang, J., Bou-Zeid, E., 2019. Scale dependence of the benefits and efficiency of green and cool roofs. Landsc. Urban Plan. 185, 127–140.
Yang, J., Wang, Z.-H., Georgescu, M., Chen, F., Tewari, M., 2016. Assessing the impact of enhanced hydrological processes on urban hydrometeorology with application to two cities in contrasting climates. J. Hydrometeorol. 17 (4), 1031–1047.
Yip, F.Y., Flanders, W.D., Wolkin, A., Engelthaler, D., Humble, W., Neri, A., Lewis, L., Backer, L., Rubin, C., 2008. The impact of excess heat events in Maricopa County, Arizona: 2000–2005. Int. J. Biometeorol. 52, 765–772.
Zonato, A., Martilli, A., Di Sabatino, S., Zardi, D., Giovannini, L., 2020. Evaluating the performance of a novel WUDAPT averaging technique to define urban morphology with mesoscale models. Urban Clim. 31, 100584.
Zonato, A., Martilli, A., Gutierrez, E., Chen, F., He, C., Barlage, M., Zardi, D., Giovannini, L., 2021. Exploring the effects of rooftop mitigation strategies on urban temperatures and energy consumption. J. Geophys. Res. Atmos. 126 (21), e2021JD035002.